Measurement of the Neutron Magnetic Form Factor

E. E. W. Bruins, Th. S. Bauer, H. W. den Bok, C. P. Duif, W. C. van Hoek,* D. J. J. de Lange,† A. Misiejuk, Z. Papandreou,‡ E. P. Sichtermann,† J. A. Tjon, H. W. Willering, and D. M. Yeomans
Universiteit Utrecht/Nationaal Instituut voor Kernfysica en Hoge-Energiefysica, P.O. Box 80000, NL-3508 TA Utrecht, The Netherlands

H. Reike,§ D. Durek, F. Frommberger, R. Gothe, D. Jakob, G. Kranefeld,‖ C. Kunz, N. Leiendecker,¶ G. Pfeiffer, H. Putsch, T. Reichelt, B. Schoch, D. Wacker, D. Wehrmeister,** and M. Wilhelm
Physikalisches Institut der Universität Bonn, Nussallee 12, D-53115 Bonn, Germany

E. Jans, J. Konijn, and R. de Vries
Sektie Kernfysica, Nationaal Instituut voor Kernfysica en Hoge-Energiefysica, P.O. Box 41822, NL-1009 DB Amsterdam, The Netherlands

C. Furget and E. Voutier
Institut des Sciences Nucléaires, IN2P3-UJF, 53 Avenue des Martyrs, F-38026 Grenoble, France

H. Arenhövel
Institut für Kernphysik, Johannes Gutenberg-Universität, D-55099 Mainz, Germany
(Received 13 January 1995)

The ratio of neutron and proton yields at quasifree kinematics was measured for the reactions $^2\mathrm{H}(e,e'n)$ and $^2\mathrm{H}(e,e'p)$ at momentum transfers $Q^2 = 0.125$, 0.255, 0.417, and 0.605 $(\mathrm{GeV}/c)^2$, detecting the neutron and the proton simultaneously in the same scintillator array. The neutron detection efficiency was measured *in situ* with the $^1\mathrm{H}(\gamma,\pi^+)n$ reaction. From this the ratio R of $^2\mathrm{H}(e,e'n)$ and $^2\mathrm{H}(e,e'p)$ cross sections was determined and used to extract the neutron magnetic form factor G_M^n in a model insensitive approach, resulting in an inaccuracy between 2.1% and 3.3% in G_M^n.

PACS numbers: 25.30.Fj, 13.40.Gp, 14.20.Dh

The electromagnetic form factors of the proton and neutron are directly related to the structure of the nucleon. Thus, they provide a testing ground for theoretical models of the subnucleonic structure of hadrons. Whereas the proton form factors are experimentally rather well established, at least for momentum transfers up to about 1 $(\mathrm{GeV}/c)^2$, this is not the case for the neutron form factors: G_E^n is subject to large uncertainties, but also G_M^n is known not better than $\pm 15\%$ [1,2]. This is not only unsatisfactory in general, but specifically recent proposals for a measurement of G_E^n are based on the spin transfer observable p_x [3,4] which yields the ratio of G_E^n and G_M^n, so that an improvement of the knowledge of G_M^n will benefit G_E^n as well. Recently, several studies have aimed at a significant improvement of G_M^n [1,5–7]. This work, a continuation of a previous study [1,5], aims at a set of G_M^n values with total uncertainties of well below 5%.

Deuterium is a suitable nuclear target for measurements on the neutron, since here the proton and neutron have identical wave functions and, due to the small binding energy, one may assume that these bound nucleons are only slightly altered from their free states. The coincident detection of the recoil neutron with the scattered electron suppresses to a large extent the dominant proton contribution.

In the experiment reported here, the ratio of the yields of the reactions $^2\mathrm{H}(e,e'n)$ and $^2\mathrm{H}(e,e'p)$ is measured for momentum transfers $Q^2 = 0.125$, 0.255, 0.417, and 0.605 $(\mathrm{GeV}/c)^2$ (kinematics I, II, III, and IV), detecting the neutron and proton simultaneously in the same scintillator array, the nucleon detector. This method, first suggested by Durand [8], was previously applied in only a few experiments [9]. In this way the luminosity, the electron detection efficiency, and the electron solid angle cancel out, while the nucleon acceptances and the choice of the deuteron wave function cancel out to first order. The layout of the experiment minimized corrections due to proton losses, and the restriction to quasifree kinematics minimized nuclear effects and their corresponding uncertainties. The hope is, hence, that systematic uncertainties can be greatly reduced compared to measurements in which only e-n coincidences or inclusive electron scattering have been applied.

The ratio R of the cross sections of the $^2\mathrm{H}(e,e'n)$ and $^2\mathrm{H}(e,e'p)$ reactions was determined after taking into account proton losses due to nuclear reactions, multiple scattering and edge effects, and an *in situ* calibration of the neutron detection efficiency. G_M^n was extracted taking into account nuclear effects, using the known e-p cross sections and available information on G_E^n. G_E^n contributes less than 2% to the e-n cross section and is not a dominant source of uncertainty.

The electron beam (between 900 and 1600 MeV, 20 to 60 nA, 20% to 50% duty cycle, depending on kinematics), delivered by the ELSA accelerator at the Physics

0031-9007/95/75(1)/21(4)$06.00

Institute at Bonn, impinged axially on a cylindrical target (length 10 cm) made from 125 μm thick kapton and filled with liquid hydrogen or deuterium. Electrons [and pions from the $^1\mathrm{H}(\gamma, \pi^+)n$ reaction] were detected in the ELAN magnetic spectrometer with four scintillators and multiwire proportional chambers and one Čerenkov counter.

Protons and neutrons were detected in the nucleon detector using the time-of-flight method. Since protons are about a hundred times more abundant than neutrons, a reliable particle identification is important. We used three thin veto scintillators which allowed a misidentification rate of far less than 10^{-4}, and the verification of the losses due to pileup [1].

For kinematics I, II, and III, the nucleon detector, which was used previously, consisted of a total of five scintillators (NE102a) of dimensions 25 $\times$ 25 cm^2 with a thickness of 2 mm for the ΔE detectors (1 mm for kinematics I) and 50 mm for the E counters. The first E counter (E_{front}) simultaneously detected protons and neutrons, while shielding behind E_{front} prevented protons from the quasielastic $^2\mathrm{H}(e, e'p)$ reaction to reach E_{back}. The neutrons detected in E_{back} were used to determine the losses in the neutron yield in E_{front} caused by the software gates on the veto detectors. For kinematics IV, the detectors of dimensions 100 $\times$ 18 cm^2 and thickness 1 and 18 cm, respectively, had a two-sided readout. At this large proton energy the use of lead to shield E_{back} becomes impracticable. We therefore installed independent veto detectors between E_{front} and E_{back} in order to determine the neutron losses. For a more detailed description see Ref. [10]. At kinematics I the nucleon detector was shielded from directly viewing the target by a 3 mm thick aluminum absorber. At kinematics IV a 5 mm thick sheet of lead was used, while at the other two momentum transfers 1 mm of lead sufficed. Each measurement of R was bracketed by two calibration runs for the neutron detection efficiency. To switch from the calibration to the measurement of the ratio, only the target and the spectrometer settings needed to be changed, which reduced the risk of systematic errors.

Neutrons detected in the nucleon detector were defined by a signal in E_{front} or in E_{back} at the correct time with respect to the spectrometer and in excess of a certain software adjustable threshold, together with a neutron condition on the veto counters. Different veto conditions on the analog to digital convertor (ADC) and time to digital convertor information were applied and used for stringent cross checks. Thanks to the duty cycle of the ELSA stretcher ring (20% to 50%), a signal to noise ratio of 200:1 for neutrons was achieved (Fig. 1).

The stability of the neutron detection efficiency of E_{front}, η_n, was monitored by means of the ADC signal for protons, and by the number of neutrons coming from the $^2\mathrm{H}(e, e'n)$ reaction scaled with the number of electrons in the spectrometer. At kinematics III and IV the $^2\mathrm{H}(\gamma, p)n$ reaction served as an additional monitor for the stability of η_n. This reaction cannot be used to determine the absolute value of η_n since pion production cannot be excluded. In addition to the coincidences between scattered electron and recoil nucleon, electron singles were recorded, prescaled to a rate of approximately 1 Hz, from which the proton yield could be determined independently.

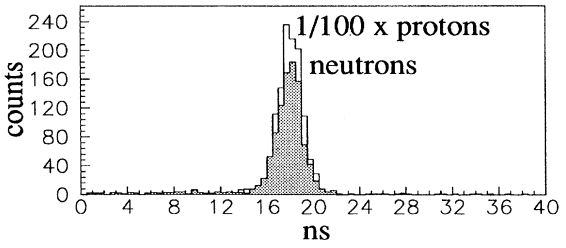

FIG. 1. Time spectra of protons (line) and neutrons (shaded area) using a subset of the data from the measurement at $Q^2 = 0.255$ (GeV/c)^2.

The reaction $^1\mathrm{H}(\gamma, \pi^+)n$ was used to obtain an *in situ, absolute* determination of the detector efficiency for neutrons. The kinematics of this reaction were arranged in such a way as to unambiguously tag neutrons impinging on the nucleon detector centered at the same energy as those from the $^2\mathrm{H}(e, e'n)$ reaction. The bremsstrahlung photons were produced in the target (and, for kinematics II, in additional radiators 40 cm upstream). The contribution of misidentified protons from the $^1\mathrm{H}(\gamma, p)\pi^0$ reaction, which contaminate the pion yield, was negligible except for kinematics II where it amounted to (3.1 $\pm$ 0.6)%. The resolution of the reaction vertex along the beam axis allowed the exclusive selection of pions for which the produced neutron was emitted in the direction of the central 8 $\times$ 6 cm^2 (6 $\times$ 50 cm^2 for kinematics IV) of E_{front} (see also Ref. [11]). For neutrons with an average energy of 61 MeV, the detection efficiency in the center of the nucleon detector as a function of threshold agreed with the one established earlier [1,5].

In order to obtain R, the measured yields must be corrected for (i) the net proton losses due to nuclear reactions and multiple scattering in the material between the reaction vertex and the detector, and (ii) the dependence of the neutron detection efficiency on the distribution of the neutrons in space and energy over the detector surface. Details about the small corrections for hydrogen contamination of the deuterium, and for the contributions of the target end caps to the different reactions, can be found in Ref. [10]. In addition, for an extraction of G_M^n one must evaluate nuclear effects, such as final state interactions (FSI), meson exchange currents (MEC), and isobar currents (IC), which alter the proton and neutron yields expected from free proton, respectively, neutron targets.

The $^1\mathrm{H}(e, e')p$ reaction was used for the determination of the proton detection efficiency, including the abovementioned losses. The experimentally found losses were

consistent with numerical checks done with the GEANT package [12] which was extended to include total proton cross sections at low energies [13]. Protons from the $^1\mathrm{H}(e,e')p$ and the $^2\mathrm{H}(e,e'p)n$ reaction were also used to calibrate and monitor the light response of the scintillators in view of the threshold dependence of the neutron detection efficiency.

The reactions $^2\mathrm{H}(e,e'n)$ and $^1\mathrm{H}(\gamma,\pi^+)n$ lead to different energy and position distributions of neutrons in E_{front}. While the neutron distribution for the $^1\mathrm{H}(\gamma,\pi^+)n$ reaction is known from experiment, the $^2\mathrm{H}(e,e'n)$ distribution was obtained using the ENIGMA Monte Carlo code [14]. The second order effect of the different distributions (including edge effects) on the ratio R was simulated with the program KSUVAX [15]. The response of the detector used for kinematics I, II, and III had been calibrated carefully previously [16] using a tagged neutron beam at PSI. The positional dependence of the response of the detector used for kinematics IV was studied by means of its double readout system.

Nuclear effects cause R to differ from the expected ratio R_{free} for free nucleons: $R_{\mathrm{free}} = R(1 - \delta R)$. The corrections δR were calculated in two different models, of which the first [17] includes FSI, MEC, and IC, and shows that FSI dominate the other corrections, whereas the second one [18] includes only FSI but is fully relativistic. It appears that the result for G_M^n obtained from R is affected to less than 0.4% by relativistic effects. Table I gives the values of δR according to the model calculations. The basic model assumptions introduce uncertainties which cannot be estimated from calculations within the framework of the model. In the absence of an exact theory such uncertainties can only be estimated by comparing the results of different models. We use the difference between the two calculations, including FSI only, as an indication of the inherent model uncertainties, and their average as the most probable correct value. To this average, we then add the effects of MEC and IC which are taken as the difference between the full calculation and the calculation including FSI only, both within the same model [17]. Since no other estimate is available, we conservatively estimate the uncertainty due to these effects to be half their size.

For the extraction of G_M^n, the e-p cross sections are needed. The measured cross section data [19] have been averaged in small intervals around the central Q^2 values, taking into account the Q^2 dependence obtained from the dipole form factors for the proton [$G_E^p = G_D = (1 + Q^2/a^2)^{-2}$, $G_M^p = 2.793 G_E^p$, and $a^2 = 0.710$ (GeV/c)^2]. The statistical errors of the data points used determine the statistical error in the average. In order to obtain the systematical error, the average has been recalculated after each e-p data set had been changed individually by its systematical errors, and adding the resulting changes quadratically. G_E^n was chosen to be 0.037 ± 0.017 [20].

The results for G_M^n, after correction for nuclear effects (Table I, Fig. 2), confirm our previous measurement at $Q^2 = 0.125$ (GeV/c)^2 and are significantly higher than that at $Q^2 = 0.093$ (GeV/c)^2. Reference [5] gives an average of G_M^n at $Q^2 = 0.093$ and 0.125 (GeV/c)^2, assuming that the ratio G_M^n/G_D is constant over this range of momentum transfer. This appears not to be the case, and the data points should not be combined into one point.

TABLE I. Statistical errors in the ratio of the neutron to proton yield Y_n/Y_p, corrections to the proton yield δY_p, and to the neutron detection efficiency $\delta\eta_n$. The cross section ratio R includes these corrections. Also given are the corrections due to nuclear effects, δR, according to two models, the average e-p cross section σ^p, and the results for G_M^n. $G_D = (1 + Q^2/a^2)^{-2}$ with $a^2 = 0.710$ (GeV/c)^2. σ_D^p is the Rosenbluth cross section using dipole proton form factors.

Kinematics	I	II	III	IV
Q^2 [(GeV/c)^2]	0.125	0.255	0.417	0.605
Stat. error Y_n/Y_p	2.7%	2.0%	3.2%	1.8%
Stat. error η_n	2.1%	2.8%	4.3%	1.3%
δY_p	(15.3 ± 0.8)%	(3.1 ± 0.1)%	(4.2 ± 0.4)%	(6.5 ± 0.8)%
$\delta\eta_n$	(6.5 ± 1.0)%	(5.0 ± 1.0)%	(7.0 ± 1.0)%	(14 ± 4)%
R	0.1333	0.2311	0.335	0.406
±stat ± syst	±0.0046 ± 0.0043	±0.0080 ± 0.0067	±0.018 ± 0.008	±0.009 ± 0.019
δR:				
Ref. [17] (FSI)	6.9%	4.3%	2.7%	5.2%
Ref. [18] (FSI)	7.1%	3.8%	2.2%	8.2%
Ref. [17] (FSI + MEC + IC)	8.5%	6.1%	3.6%	5.8%
σ^p/σ_D^p	0.944	0.946	0.957	0.975
±stat ± syst	±0.003 ± 0.012	±0.003 ± 0.019	±0.004 ± 0.016	±0.005 ± 0.027
G_E^n	0.037 ± 0.017	0.037 ± 0.017	0.037 ± 0.017	0.037 ± 0.017
G_M^n	−1.411	−1.114	−0.862	−0.616
±stat ± syst	±0.025 ± 0.021	±0.020 ± 0.014	±0.025 ± 0.013	±0.008 ± 0.018
$G_M^n/(-1.913 G_D)$	1.020	1.076	1.135	1.104
±stat ± syst	±0.018 ± 0.015	±0.019 ± 0.013	±0.033 ± 0.017	±0.014 ± 0.032

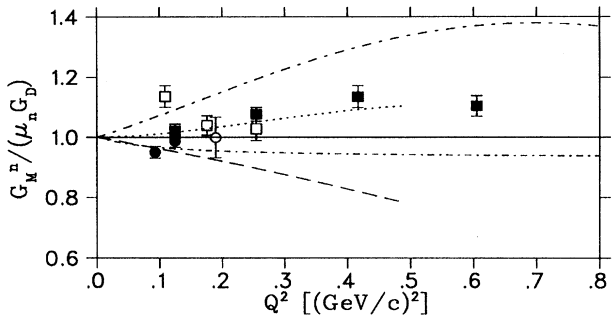

FIG. 2. Data from recent G_M^n measurements up to $Q^2 = 0.8$ $(\mathrm{GeV}/c)^2$, scaled to the dipole fit: black circles [5], open squares [6], and open circle [7]. The black squares are from this work. Several model predictions are shown. VMD: The minimal (dotted line) and complete (long dashed) model of [21]. Constituent quark model: nonrelativistic calculation of [22] (dot-long dashed), relativistic calculation of [23] (dot-short dashed).

Recently Markowitz *et al.* [6] determined G_M^n from an absolute measurement of the $^2\mathrm{H}(e, e'n)$ cross section. At 0.109 $(\mathrm{GeV}/c)^2$, their result lies 13.6% above the dipole fit, whereas our result at 0.125 $(\mathrm{GeV}/c)^2$ is only 2.5% above. Relativistic effects, which have not been applied in [6], do not appear to remove this discrepancy. Our results agree with the other results of [6], and with the result obtained by Gao *et al.* [7] using polarization techniques. Figure 2 shows that most of the recent theoretical predictions of G_M^n are not in agreement with our data (fits to G_M^n data have not been included). The only model which reproduces the trend indicated by the data is the minimal model of Meissner [21].

In conclusion, we have combined the ratio method proposed long ago with the possibilities offered only recently by the large duty cycle electron beams to measure G_M^n with substantially decreased uncertainties. The coincident detection of the electron and the knocked out nucleon significantly reduces uncertainties due to nuclear effects, whereas the large duty cycle allows us to detect simultaneously protons and neutrons. It would be of interest to extend the range of high precision determinations of G_M^n to higher momentum transfers, where only inclusive electron scattering data exist, but where the selectivity to models increases.

We would like to thank D. N. van Dierendonck, E. J. B. Maas, and J. Voets for their help during the experiment. The Dutch authors are grateful to the staff of the ELSA accelerator for their hospitality and their help during the experiment. This work was supported by the Stichting voor Fundamenteel Onderzoek der Materie, the Bundesministerium für Forschung und Technologie, and the Deutsche Forschungsgemeinschaft (SFB 201).

*Present address: Katholieke Universiteit/NIKHEF-H, Nijmegen, The Netherlands.
†Present address: Vrije Universiteit/NIKHEF-K, Amsterdam, The Netherlands.
‡Present address: Department of Physics, The George Washington University, Washington, DC 20052.
§Present address: Mannesmann Mobilfunk, Düsseldorf, Germany.
‖Present address: Deutsche Goodyear, Köln, Germany.
¶Present address: Gruner & Jahr, Itzehoe, Germany.
**Present address: Colonia Versicherung, Köln, Germany.

[1] F. C. P. Joosse, Ph.D. thesis, Universiteit Utrecht; D. Fritschi, Ph.D. thesis, Universität Basel, 1993.
[2] E. E. W. Bruins and Th. S. Bauer (to be published).
[3] J. Scofield, Phys. Rev. **113**, 1599 (1959); **141**, 1352 (1966); N. Dombey, Rev. Mod. Phys. **41**, 236 (1969); R. G. Arnold, C. E. Carlson, and F. Gross, Phys. Rev. C **23**, 363 (1981).
[4] K. Lee *et al.,* Phys. Rev. Lett. **70**, 738 (1993).
[5] H. Anklin *et al.,* Phys. Lett. B **336**, 313 (1994).
[6] P. Markowitz *et al.,* Phys. Rev. C **48**, R5 (1993).
[7] H. Gao *et al.,* Phys. Rev. C **50**, R546 (1994).
[8] L. Durand, Phys. Rev. **115**, 1020 (1959); **123**, 1393 (1961).
[9] W. Bartel *et al.,* Phys. Lett. **30B**, 285 (1969); **39B**, 407 (1972).
[10] E. E. W. Bruins, Ph.D. thesis, Universiteit Utrecht (unpublished).
[11] H. Reike, Ph.D. thesis, Universität Bonn, 1993.
[12] CERN Computer Newsletter **200**, 13 (1990).
[13] Z. Papandreou, Int. Rep., Universiteit Utrecht, 1992.
[14] J. L. Visschers, in *MC93,* edited by P. Dragovitsch, S. L. Linn, and M. Burbank (World Scientific, Singapore, 1994), p. 350.
[15] R. A. Cecil, B. D. Anderson, and R. Madey, Nucl. Instrum. Methods **161**, 439 (1979).
[16] M. Loppacher, Diplomarbeit, Universität Basel, 1992.
[17] H. Arenhövel, W. Leidemann, and E. L. Tomusiak, Phys. Rev. C **46**, 455 (1992).
[18] E. Hummel and J. A. Tjon, Phys. Rev. C **49**, 21 (1994).
[19] Data compilation by J. Jourdan (private communication).
[20] S. Platchkov *et al.,* Nucl. Phys. **A510**, 740 (1990).
[21] U.-G. Meissner, Phys. Rep. **161**, 213 (1988).
[22] M. Warns *et al.,* Z. Phys. C **45**, 627 (1990).
[23] F. Schlumpf, J. Phys. G **20**, 237 (1994).